SUPPLEMENTAL INFORMATION

Deficiency of asparagine synthetase causes congenital microcephaly and a progressive form of encephalopathy.

Table of Contents

SUPPLEMENTAL INFORMATION

Deficiency of asparagine synthetase causes congenital microcephaly and a progressive form of encephalopathy.

SUPPLEMENTAL DATA: FIGURES

Figure S1. Brain MRIs from additional families. (Relates to Figure 2: MRI images from family C)

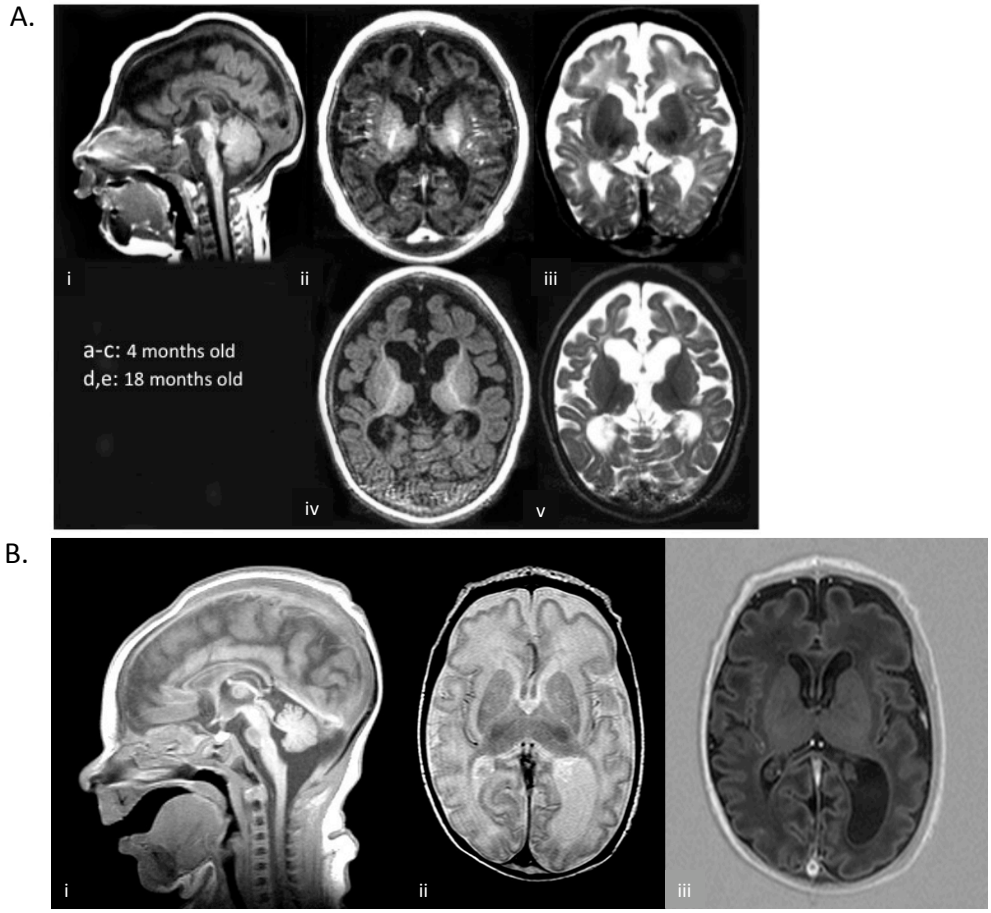

Figure S1A. Brain MRI from patient A.II.1. MRI from individual A.II.1 in family A. T1W sagittal image **(i)** at 4 months of age demonstrates micrognathia, sloping forehead, thin brainstem and relatively normal cerebellum. T1 axial image **(ii)** reveals severe cortical and subcortical atrophy and delay in myelin maturation, with myelin only in the posterior limbs of internal capsule. T2 axial image **(iii)** reveals abnormally increased signal intensity of the white matter for age, prominent ventricles and pericerebral spaces over the frontal convexity. T1W axial image **(iv)** at 18 months of age confirms persistent myelin delay and parenchymal volume loss. Concurrent T2W axial image **(v)** shows abnormal signal and atrophy of the white matter, progressive ventriculomegaly and pericerebral spaces due to volume loss. **Figure S1B. Brain MRI from patient D.II.2. (i)** Sagittal T1 image showing small pons. **(ii)** Axial T2 image showing decreased brain volume, delayed myelin maturation, and simplified gyral pattern predominantly in the frontal regions. **(iii)** Axial T1 image confirming the delayed myelination and the other findings seen on the Axial T2 image.

SUPPLEMENTAL INFORMATION

Deficiency of asparagine synthetase causes congenital microcephaly and a progressive form of encephalopathy.

Figure S2. In vitro ASNS characterization. (Relates to Figure 3: Functional impact of ASNS mutations)

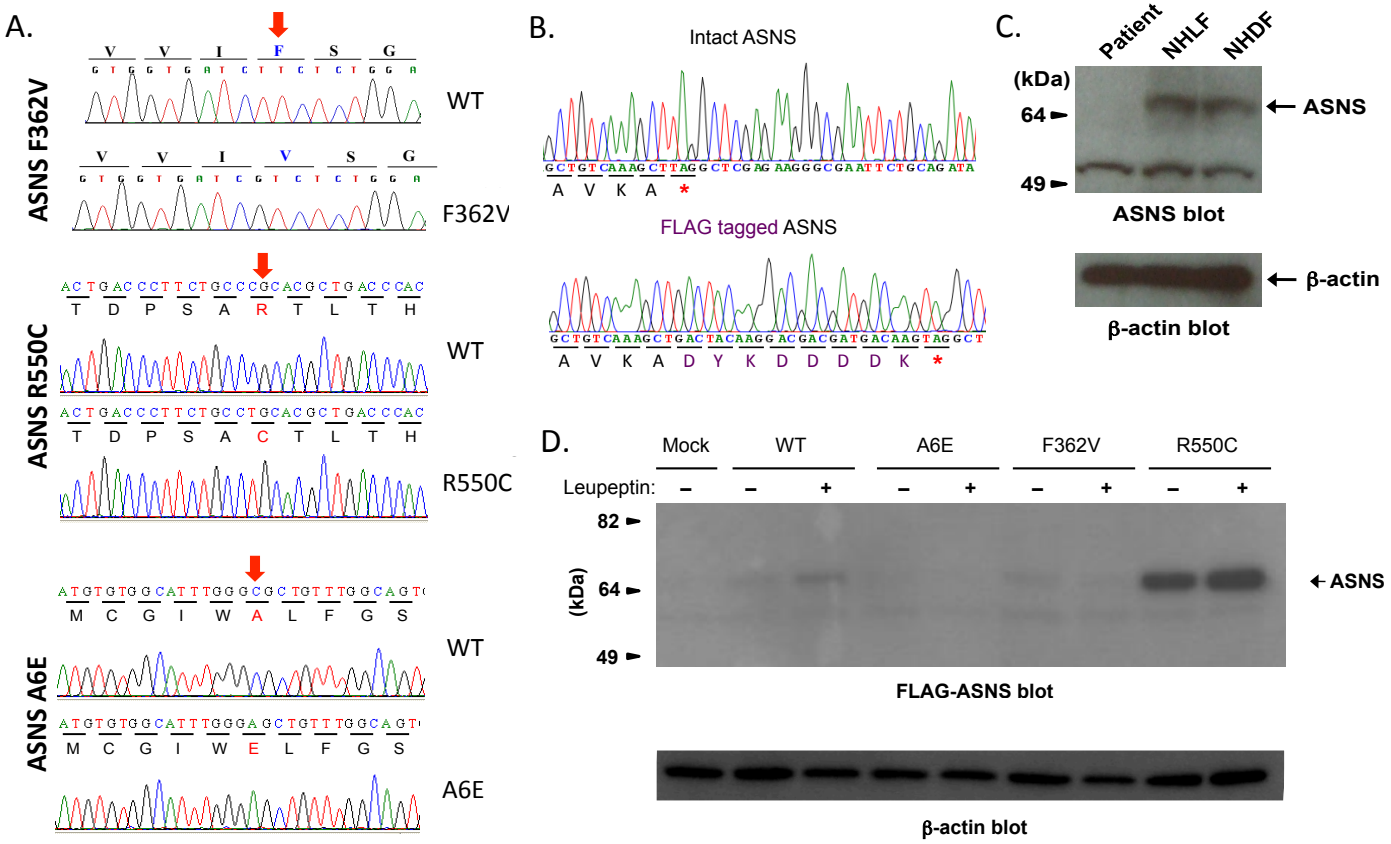

Figure S2A. Sanger sequencing of *in vitro ASNS* alleles. After PCR-directed mutagenesis, cDNA encoding human *ASNS* containing wild type or mutant alleles was subcloned into pcDNA3.1(+) vector and subjected to sequence analysis. **Figure S2B. Sanger sequencing of FLAG-tagged *ASNS*.** A FLAG-tag was introduced into the sequence encoding the C-terminus of ASNS for the wild type and the three mutant forms (A6E, R550C and F362V) and subjected to sequence analysis. **Figure S2C. ASNS levels in patient fibroblast cells.** ASNS in a patient with the F362V mutation (Family A: II.1) was detected using an anti-ASNS antibody. NHDF and NHLF are human fibroblast cell lines. The protein in the patient cells is depleted as was seen with the *in vitro* mutagenesis studies. **Figure S2D. ASNS levels in COS-7 cells transfected with empty, wild-type, or mutant vectors.** Western Blots detecting ASNS-FLAG protein abundance, with or without Leupeptin treatment, in COS-7 transfectants using an anti-FLAG antibody. β-actin was used as a loading control.

SUPPLEMENTAL INFORMATION

Deficiency of asparagine synthetase causes congenital microcephaly and a progressive form of encephalopathy.

Figure S3. ASNS expression in different tissues and the developing mouse brain. (Relates to Figure 5: Asns deficient mouse and structural brain abnormalities)

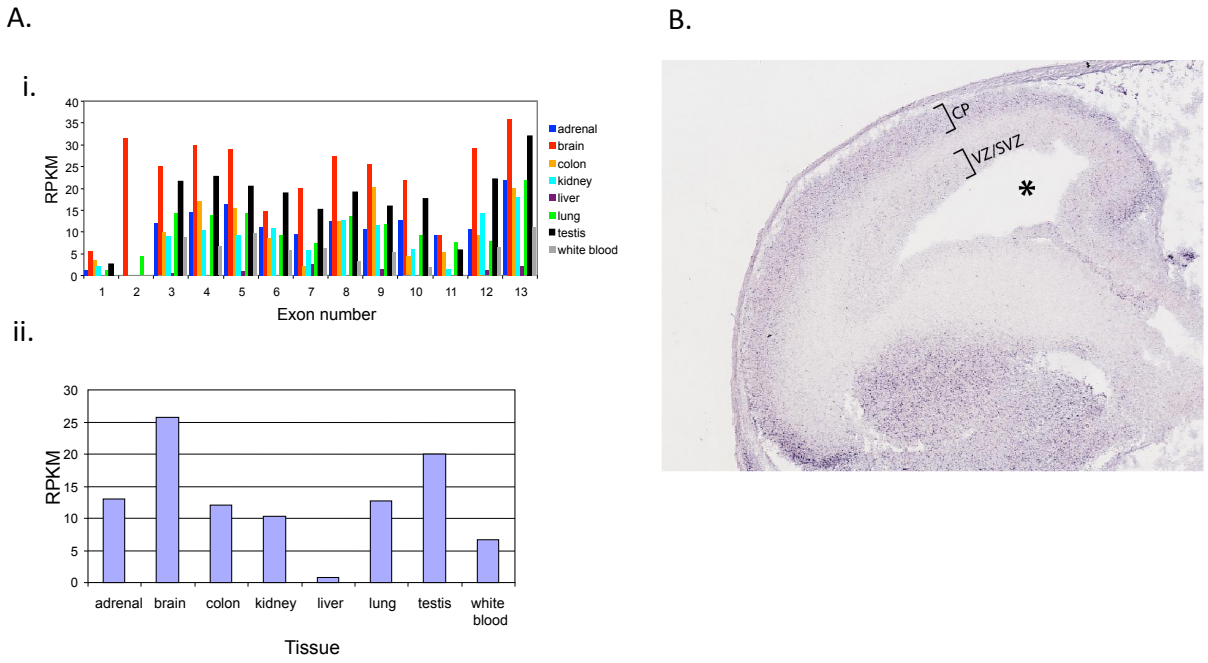

Figure S3A. *ASNS* expression in different tissues. Expression profile of *ASNS* gene (ENST00000394308) using RNA-seq data, extracted from the Human Body Map 2.0 Project of Illumina (downloadable from Integrative Genomics Viewer (IGV) at http://www.broadinstitute.org/igv/). In this database, the RNA from each tissue was obtained from a single individual. Extracted reads were aligned to the human genome (hg19) using Bowtie(Langmead et al., 2009), and BEDTools(Quinlan and Hall, 2010) was applied for counting the number of reads per exon. Data were normalized to reads per kilobase of exon model per million mapped reads (RPKM) values. (i) Normalized expression per exon, showing an indication of brain-specific expression of exon 2. (ii) Normalized expression for the whole gene. The finding that *ASNS* is more highly expressed in brain and testis is in agreement with Horowitz *et al.*(Horowitz et al., 1968). **Figure S3B. *Asns* expression in the developing mouse brain.** *Asns* mRNA *in situ* hybridization of the developing mouse brain (sagittal section) at E14.5. *Asns expression* is particularly enriched in the cortical plate (CP) and ventricular and sub-ventricular zone layers (VZ/SVZ). The asterisk is labeling the ventricle of the developing mouse cerebral cortex. *In situ* images were taken from (http://www.eurexpress.org/, euxassay_004453)[22].

SUPPLEMENTAL INFORMATION

Deficiency of asparagine synthetase causes congenital microcephaly and a progressive form of encephalopathy.

Figure S4. Asns knock out mouse details and phenotyping. (Relates to Figure 5: Asns deficient mouse and structural brain abnormalities)

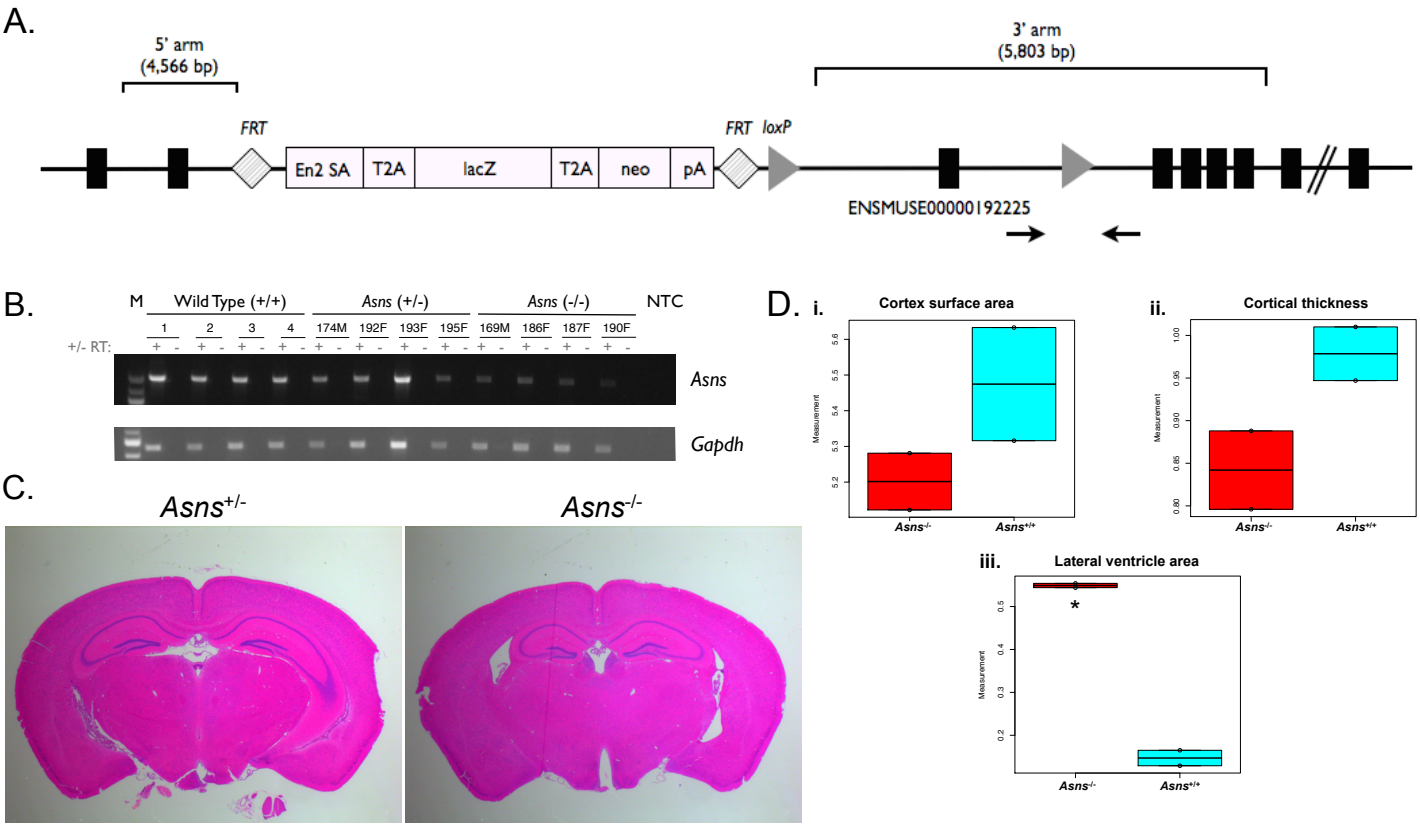

Figure S4A. Construct for knocking out *Asns* and genotyping primers. We obtained genetically modified mice from EMMA (http://www.emmanet.org/strains.php). This diagram shows the complete construct including the with a splice acceptor site, after exon 2, for the lacZ gene (B6NTac;B6N-Asns$^{tm1a(EUCOMM)Wtsi}$/H). Mice were genotyped using the following custom primer sequences (black arrows): forward: 5'-TTT TGG TTT GTG TTT CTT CCT G-3' and reverse: 5'-TCA GGA ACG TGA GTG AGT GAG T-3'. **Figure S4B. *Asns* adult mouse brain RT-PCR exons 2-12.** *Asns* RT-PCR with low cDNA input (250ng) and PCR cycle (35 cycles) was used to assess the existence of *Asns* mRNA transcripts semi-quantitatively. RT-PCR spanned from exon 2 to exon 12 using the specific primer set: 5'- CAG TGT CTG AGT GCG ATG AAG A -3' and 5'- GCG TTC AAA GAT CTG ACG GTA G-3'. *Gapdh* RT-PCR with low cDNA input (250ng) and PCR cycle (25 cycles) was used as a control using the specific primer set: 5'-ACC ACA GTC CAT GCC ATC AC-3' and 5'-CAC CAC CCT GTT GCT GTA GCC-3'**. Figure S4C. Asns adult mouse brain sections.** Coronal sections from one homozygous mutant mouse (-/-) and an age matched (P84) heterozygous littermate (+/-). **Figure S4D. Postnatal day zero (P0) mouse brain measurements.** Measurements were taken using two homozygous mutant mouse and two age matched (P0) wild type littermates. (i) Surface area of the mouse cortex (right hemisphere only) (ii) cortical thickness and (iii) Lateral ventricle area of right hemisphere; * indicates a significant difference by an unpaired t-test (p=0.019). Measurement units are arbitrary.

SUPPLEMENTAL INFORMATION

Deficiency of asparagine synthetase causes congenital microcephaly and a progressive form of encephalopathy.

Figure S5. Behavioral analyses of Asns mice. (Relates to Figure 5: Asns deficient mouse and structural brain abnormalities)

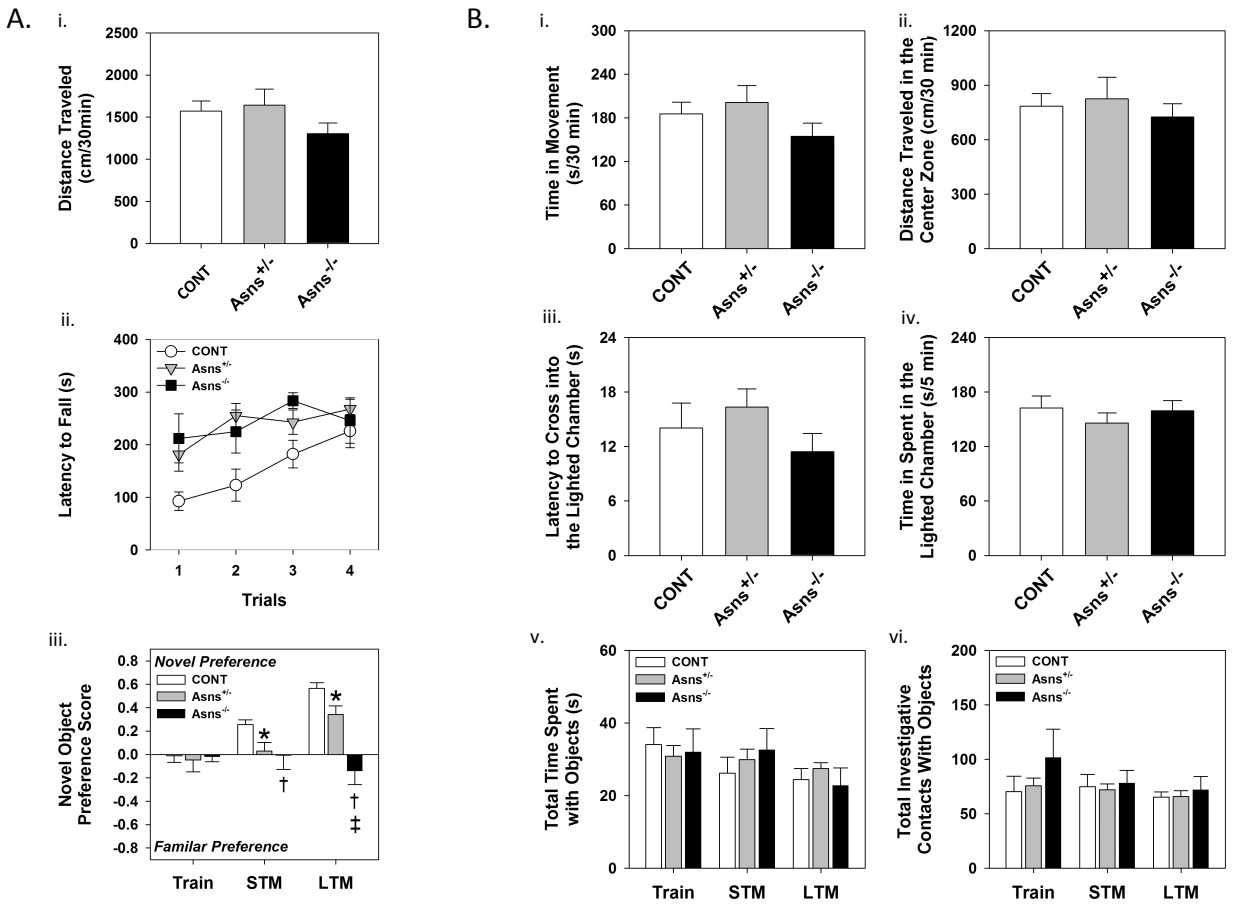

Figure S5A. Behavioral analyses of Asns mice. (i) Spontaneous locomotor activity in the open field over 30 min for B6NTac control (CONT), Asns$^{+/-}$, and Asns$^{-/-}$ mice. (ii) Latency to fall from the rotorod across four trials. (iii) Preference scores from the novel object recognition test as assessments during training (Train), short-term (STM), and long-term memory. N=8 CONT, 11 Asns$^{+/-}$, and 6 Asns$^{-/-}$ mice. *p<0.05, CONT versus Asns$^{+/-}$ mice, †p<0.05, CONT versus Asns$^{-/-}$mice, ǂp<0.05, Asns$^{+/-}$ versus Asns$^{-/-}$ mice. **Figure S5B. Behavioral analysis of CONT, Asns$^{+/-}$, and Asns$^{-/-}$ Mice.** (i) Time in movement in the open field. (ii) Distance traveled in the center zone of the open field. (iii) Latency to enter the lighted chamber in the light-dark emergence test. (iv) Time spent in the lighted chamber in the light-dark emergence test. (v) Total time spent with objects in the novel object recognition test. (vi) Total investigative contacts with objects. STM = short-term memory, LTM = long-term memory. N=8 CONT, 11 Asns$^{+/-}$, and 6 Asns$^{-/-}$ mice.

SUPPLEMENTAL INFORMATION

Deficiency of asparagine synthetase causes congenital microcephaly and a progressive form of encephalopathy.

SUPPLEMENTAL DATA: TABLES

Table S1. All rare variants shared in both patients from family B. (Relates to Table 2: Mutations identified in ASNS)

Functional category	Homozygous	Heterozygous
Essential splice site	1	2
Intron-exon boundary (SNV)	10	32
Intron-exon boundary (indel)	1	9
Non-synonymous coding	58	248
Stop gained	1	5
Coding-disrupted frameshift (indel)	1	8
Coding-disrupted other (indel)	0	2
Total	72	306

Table S1. All rare variants shared in both patients from family B. A summary of all rare variants, with a plausible impact on the function of the resulting gene product, shared in family B (found in both affected individuals Fig. 1a: II.2 and II.4). A rare variant was defined as having a predicted homozygote frequency of ≤ 3% in the population of 261 sequenced control genomes.

Table S2. All rare homozygous functional variants found in both patients from family B. (Relates to Table 2: Mutations identified in ASNS)

Variant	Variant ID	Variant type	Gene symbol	Variant frequency	Variant	Variant ID	Variant type	Gene symbol	Variant frequency
1	7_97322654_C	SNV	ASNS	0.000	37	9_39075808_C	SNV	CNTNAP3	0.117
2	7_107186210_T	SNV	CBLL1	0.000	38	19_38355194_C	SNV	WDR88	0.119
3	7_107475774_C	SNV	LAMB4	0.000	39	19_59416242_A	SNV	LILRB3	0.119
4	7_106296855_T	SNV	PIK3CG	0.002	40	22_44146055_T	SNV	SMC1B	0.121
5	6_41721834_A	SNV	MDFI	0.004	41	X_1497953_T	SNV	ASMTL	0.121
6	12_51248317_A	SNV	KRT74	0.006	42	12_48631243_A	SNV	AQP2	0.123
7	7_106725874_C	SNV	COG5	0.008	43	16_2045401_T	SNV	TSC2	0.123
8	19_38307917_T	SNV	GPATCH1	0.010	**44**	15_19884068_C	SNV	OR4N4	0.123
9	7_104993051_A	SNV	RINT1	0.012	45	6_32740678_A	SNV	HLA-DQB1	0.125
10	7_98997458_G	SNV	ZNF655	0.015	46	22_29862960_T	SNV	PLA2G3	0.127
11	12_51152337_G	SNV	KRT6C	0.025	47	X_1500706_G	SNV	ASMTL	0.127
12	17_35550980_DEL_T	indel	CASC3	0.031	48	17_27649318_A	SNV	RHBDL3	0.129
13	16_2100974_G	SNV	PKD1	0.044	49	X_1506842_G	SNV	ASMTL	0.129
14	17_41416696_G	SNV	MAPT	0.046	50	11_77586662_A	SNV	USP35	0.131
15	7_107004256_A	SNV	DUS4L	0.048	51	22_30919090_T	SNV	RFPL2	0.131
16	6_24511434_T	SNV	MRS2L	0.050	**52**	19_59416243_A	SNV	LILRB3	0.135
17	18_12244956_A	SNV	CIDEA	0.054	53	16_2105631_C	SNV	PKD1	0.137
18	7_102361951_G	SNV	LRRC17	0.054	54	20_10551750_A	SNV	C20orf94	0.138
19	12_51838742_G	SNV	CSAD	0.056	55	3_41852418_C	SNV	ULK4	0.142
20	7_102452856_G	SNV	FBXL13	0.056	56	14_20569961_T	SNV	TPPP2	0.146
21	19_38209355_T	SNV	RHPN2	0.060	57	1_151037145_A	SNV	LCE1D	0.148
22	7_101885015_A	SNV	ALKBH4	0.062	**58**	12_51503256_A	SNV	KRT79	0.148
23	19_13901896_A	SNV	CC2D1A	0.079	59	1_37961428_A	SNV	EPHA10	0.160
24	16_2102362_G	SNV	PKD1	0.083	60	10_18868641_G	SNV	CACNB2	0.160
25	16_2095427_C	SNV	PKD1	0.087	**61**	7_29127129_T	SNV	CPVL	0.162
26	7_99655521_T	SNV	PVRIG	0.102	62	19_37859295_T	SNV	RGS9BP	0.162
27	1_37958776_T	SNV	EPHA10	0.104	63	15_41604696_A	SNV	MAP1A	0.163
28	7_100324690_C	SNV	UFSP1	0.104	64	16_2092388_G	SNV	PKD1	0.165
29	8_17202048_G	SNV	MTMR7	0.104	65	6_31432179_C	SNV	HLA-B	0.169
30	18_59805277_G	SNV	SERPINB8	0.104	**66**	15_19884261_G	SNV	OR4N4	0.169
31	3_62164229_A	SNV	PTPRG	0.108	67	1_75475262_A	SNV	SLC44A5	0.171
32	1_159963696_C	SNV	FCRLB	0.110	68	2_111315429_T	SNV	ACOXL	0.171
33	6_109430212_T	SNV	SESN1	0.110	69	11_77598578_G	SNV	USP35	0.173
34	X_152517671_INS_C	indel	FAM58A	0.112	70	3_47427122_A	SNV	PTPN23	0.175
35	12_51330534_T	SNV	KRT2	0.115	71	2_238675316_C	SNV	ESPNL	0.179
36	6_109587255_C	SNV	C6orf182	0.117	72	17_35133114_G	SNV	ERBB2	0.179

Table S2. All rare homozygous functional variants found in both patients from family B. The 72 homozygous functional variants found in both II.2 and II.4 of family B. The variants are listed in ascending order based on the variant allele frequency in the sequenced control population. The bolded variant numbers denote the 9 variants that were also observed in the affected individual from family A (Fig. 1a, II.1).

SUPPLEMENTARY INFORMATION

Deficiency of asparagine synthetase causes congenital microcephaly and a progressive form of encephalopathy.

Table S3. Regions of shared homozygosity in Family C. (Relates to Table 2: Mutations identified in ASNS)

Chr	Marker start	Marker end	Position start	Position end	Size (Mb)
1	rs3863722	rs272822	35,592,376	36,677,585	1.1
1	rs319950	rs9436447	49,091,687	50,590,732	1.5
3	rs3895736	rs3197999	48,658,467	49,721,532	1.1
3	rs9790150	rs2882429	133,723,028	139,835,865	6.1
4	rs10517277	rs6858830	33,466,803	34,500,856	1.0
5	rs10477652	rs10478752	123,179,118	126,087,378	2.9
7	rs11773446	rs7780168	95,944,485	131,291,677	35.3
12	rs1564121	rs12311684	86,138,548	89,435,177	3.3

Table S3. Regions of shared homozygosity (>1Mb) between the affected individuals in Family C (II.3 and II.4).

Table S4. Exome sequencing variant filtering in family C. (Relates to Table 2: Mutations identified in ASNS)

Filter	Remaining variants
Coding /Splicing	20,439
Remove synonymous (non-splicing)	10,175
Rare*	856
Homozygous	25
In homozygous region	3
Segregating with the disease in the homozygous state	ASNS:NM_183356:exon14:c.C1648T:p.R550C CYP3A4:NM_017460:exon12:c.G1282A:p.D428N
Predicted damaging (SIFT or polyphen-2)	ASNS:NM_183356:exon14:c.C1648T:p.R550C

Table S4. Exome sequencing variant filtering in family C. *Rare variants were defined as those present at a frequency ≤3% in in-house control exomes (n=169), 1,000 genomes, and NHLBI Exome Sequencing Project.

SUPPLEMENTAL INFORMATION

Deficiency of asparagine synthetase causes congenital microcephaly and a progressive form of encephalopathy.

Table S5. Exome sequencing variant filtering in family D. (Relates to Table 2: Mutations identified in ASNS)

	Affected males		Unaffected male	Unaffected female
	II.1	II.2	II.4	II.5
Coding/Splicing	20,336	21,120	19,325	20,252
Remove synonymous (non-splicing)	10,021	10,491	9,793	10,363
Shared by II.1 and II.2	7,830			
Rare*	237			
Homozygous in II.1 & II.2 but *not* homozygous in II.4 or II.5	0			
Variants on chr X in II.1 and II.2 but not in II.4	0			
Genes with ≥2 rare variants in common to II.1 & II.2	14			
Genes with ≥2 rare variants in common to II.1 & II.2 but not in common with II.4 or II.5 (*compound heterozygous*).	ASNS (NM_183356) c.C1648T:p.R550C c.C17A:p.A6E			

Table S5. Exome sequencing variant filtering in family D. Rare variants were defined as those present at a frequency ≤3% in in-house control exomes (n=169), 1000 genomes, and NHLBI Exome Sequencing Project.

Table S6. F362V ASNS shared haplotype in families A and B. (Relates to Table 2: Mutations identified in ASNS)

SNV	Coordinate	Alleles
1	chr7:97322654	C/C
2	chr7:97325666	A/A
3	chr7:97326505	T/T
4	chr7:97621997	C/C
5	chr7:97654263	T/T
6	chr7:97660051	A/A
7	chr7:97660146	A/A
8	chr7:97760787	T/T
9	chr7:97760811	A/A
10	chr7:97771537	T/T
11	chr7:97782680	A/A
12	chr7:98298760	A/A
13	chr7:98338892	T/T
14	chr7:98396816	C/C
15	chr7:98487987	C/C
16	chr7:98488035	C/C

Table S6. The shared F362V *ASNS* haplotype in families A and B. The 16 variants found in the shared p.F362V *ASNS* haplotype. The first SNV is the *ASNS* p.F362V variant.

SUPPLEMENTAL INFORMATION

Deficiency of asparagine synthetase causes congenital microcephaly and a progressive form of encephalopathy.

Table S7. Summary of exome-sequencing coverage in homozygous regions. (Relates to Table 2: Mutations identified in ASNS)

Individual	# of genes with ≥70% bases covered	# of genes with <70% of bases covered	Average % of bases covered
Family A (II-1)	600	72	89.03%
Family B (II-2)	601	71	89.01%
Family B (II-4)	602	70	89.01%

Table S7. Summary of exome-sequencing coverage in homozygous regions. There are 672 HGNC recognized protein-coding genes found either partially or fully within the predicted shared homozygous regions (n=170, present in all sequenced patients from Families A and B). All known Ensembl exons(Hubbard et al., 2009), excluding UTRs, were then assessed for coverage, where a base is considered covered if ≥5 short-reads spanned this nucleotide. Each sequenced sample has ≥600 of these genes with ≥70% of their bases covered and each sample averages nearly 90% nucleotide coverage across these 672 genes.

Table S8. Seven primary microcephaly loci. (Relates to Table 2: Mutations identified in ASNS)

Locus	Location	Gene	Coordinates (NCBI36)	MIM
MCPH1	8p23	Microcephalin (MCPH1)	chr8:6,251,529-6,493,434	607117
MCPH2	19q13	WD repeat-containing protein 62 (WDR62)	chr19:41,237,623-41,245,393	613583
MCPH3	9q33	CDK5 regulatory subunit-associated protein 2 (CDK5RAP2)	chr9:122,190,968-122,250,225	608201
MCPH4	15q21	Centrosomal protein, 152-KD (CEP152)	chr15:37,900,001-42,700,000	613529
MCPH5	1q31	Abnormal spindle-like, microcephaly-associated (ASPM)	chr1:195,319,997-195,382,287	605481
MCPH6	13q12	Centromeric protein J (CENPJ)	chr13:24,354,412-24,395,085	609279
MCPH7	1p32	SCL/TAL1-interrupting locus (STIL)	chr1:47,488,398-47,552,406	181590

Table S8. Seven primary microcephaly loci. The previously identified primary microcephaly loci and associated information about casual gene at each loci.

SUPPLEMENTAL INFORMATION

Deficiency of asparagine synthetase causes congenital microcephaly and a progressive form of encephalopathy.

Table S9. Predicted homozygous regions overlapping known primary microcephaly loci. (Relates to Table 2: Mutations identified in ASNS)

Individual	Homozygous region start coordinate	Overlap gene	Overlap start coordinate	Overlap stop coordinate	Size of overlap (KB)
Family A (II-1)	chr13:24181657	CENPJ	24354412	24395085	40.674
Family B (II-4)	chr8:6259807	MCPH1	6259807	6364841	105.035
Family A (II-1)	chr8:6289591	MCPH1	6289591	6466364	176.774
Family A (II-1)	chr9:122210554	CDK5RAP2	122210554	122250225	39.672

Table S9. Predicted homozygous regions overlapping known primary microcephaly loci. Four regions of homozygosity were identified by the PLINK program(Purcell et al., 2007) that overlap one of the known microcephaly loci. None of these regions were found in more than one of the three case genomes.

Table S10. Sequencing coverage for exome-sequenced samples from families A-D. (Relates to Table 2: Mutations identified in ASNS)

Individual	Total covered bases (MB)	% covered bases	Average read depth
Family A (II-1)	36.32	96.1	79.92
Family B (II-2)	36.30	96.0	63.93
Family B (II-4)	36.21	95.8	69.59
Family C (II-3)	51.28	95.0	80
Family D (II-1)	51.64	97.5	144
Family D (II-2)	51.37	95.8	126
Family D (II.4)	51.53	96.3	128
Family D (II.5)	51.67	97.8	89

Table S10. Sequencing coverage for each of the exome-sequenced samples from families A-D. A base within the 37.8Mb (families A and B) or the 52 Mb captured region (families C and D) is defined as covered if ≥5 short-reads spanned this nucleotide. After accounting for PCR duplicates and reads that did not align to captured regions of the reference genome, the average read depth for each sample was greater than 63x and greater than 95% of targeted bases were covered in all eight samples.

SUPPLEMENTAL INFORMATION

Deficiency of asparagine synthetase causes congenital microcephaly and a progressive form of encephalopathy.

Table S11. Enzymes of the alanine, aspartate, and glutamine metabolic pathway and associated OMIM disorders. (Relates to Table 3: Measurements of amino acid concentrations in patient blood and urine)

Enzyme	Gene	Associated OMIM disorder	OMIM disorder number	Neurological impairments
1.2.1.24	ALDH5A1	Succinic semialdehyde dehydrogenase deficiency	#271980	yes
1.4.1.3	GLUD1	Hyperinsulinism-hyperammonemia syndrome	#606762	yes
1.4.3.1	DDO	No disease associations in OMIM	-	no
1.4.3.2	IL4I1	No disease associations in OMIM	-	no
1.5.1.12	ALDH4A1	Hyperprolinemia, type II	#239510	yes
2.1.3.2	CAD	No disease associations in OMIM		no
2.4.2.14	PPPAT	No disease associations in OMIM	-	no
2.6.1.1	GOT1	No proven disease associations in OMIM	#614419	no
2.6.1.16	GFPT1	Myasthenia, congenital, with tubular aggregates 1	#610542	no
2.6.1.19	ABAT	GABA-transaminase deficiency	#613163	yes
2.6.1.2	GPT	No disease associations in OMIM	-	no
2.6.1.44	AGXT	Hyperoxaluria, primary, type 1	#259900	no
3.5.1.15	ASPA	Canavan disease	#271900	yes
3.5.1.2	GLS2	No disease associations in OMIM	-	no
3.5.1.3	NIT2	No disease associations in OMIM	-	no
4.1.1.15	GAD1	Cerebral palsy, spastic quadriplegic, 1	#603513	yes
4.3.2.1	ASL	Argininosuccinic aciduria	#207900	yes
4.3.2.2	ADSL	Adenylosuccinase deficiency	#103050	yes
6.3.1.2	GLUL	Glutamine deficiency, congenital	#610015	yes
6.3.4.16	CPS1	Carbamoylphosphate synthetase I deficiency	#237300	yes
6.3.4.4	ADSSL1	No disease associations in OMIM	-	no
6.3.4.5	ASS1	Citrullinemia	#215700	yes
6.3.5.4	ASNS	No disease associations in OMIM		yes
6.3.5.5	CAD	No disease associations in OMIM	-	no

Table S11. The identification of *ASNS* as the disease-causing gene in our patients also highlights the importance of human enzymes in the alanine, aspartate, and glutamine metabolic pathway in neurodevelopmental disorders. Human enzymes in the alanine, aspartate, and glutamine metabolic pathway (http://www.genome.jp/kegg-bin/show_pathway?hsa00250) and their associated OMIM disorders.

SUPPLEMENTAL INFORMATION

Deficiency of asparagine synthetase causes congenital microcephaly and a progressive form of encephalopathy.

SUPPLEMENTARY EXPERIMENTAL PROCEDURES

Comparison to MCPH genes

Despite congenital microcephaly being a consistent feature of this syndrome, our patients do not fit the definition of primary microcephaly (MCPH). MCPH disorders are characterized by: a profoundly small head at birth, modest developmental delay (considering the dramatic microcephaly), mild or no seizures, and little or no deterioration. To date, there are seven distinct chromosomal loci for autosomal recessive primary microcephaly: MCPH1-MCPH7 (MIM 251200, 604317, 604804, 604321, 608716, 608393, and 612703, respectively). The causal genes have been identified for all of these loci (Table S8), including the recent discoveries of causal genes in MCPH2(Bilguvar et al., 2010; Nicholas et al., 2010) and MCPH4(Guernsey et al., 2010). Multiple types of casual mutations (e.g., non-synonymous, small deletions) have been identified in each of these genes(Bilguvar et al., 2010; Guernsey et al., 2010; Kaindl et al., 2010; Nicholas et al., 2010). The observed genetic heterogeneity is not surprising given the broad clinical spectrum of primary microcephaly(Cox et al., 2006).

However, since we still wanted to exclude the possible involvement of previously identified primary microcephaly genes (Table S8), these loci were analyzed with respect to the 1,532 homozygous regions identified in any of the three case genomes (families A and B). There were four homozygous regions that overlapped one of the microcephaly-associated genes, however these regions were never homozygous in more than one patient (Table S9). Parenthetically, exome sequencing has the potential to miss casual variants if the exon harboring it is not captured or if there is undetectable structural variation. Our analysis, however, suggests that homozygous variants on a single haplotype have not been missed in any of the microcephaly genes.

The new syndrome most resembles a host of neurometabolic disorders(Hart et al., 2007; Kelley et al., 2002; Siu et al., 2010) that show microcephaly at birth and progressive deterioration, including progressive brain atrophy. Amish microcephaly (MCPHA, OMIM #607196) is one of the most well-defined examples of a metabolic disorder which resembles the new syndrome. MCPHA is characterized by infantile microcephaly and α-ketoglutaric aciduria. However, we noted that Amish microcephaly is more severe than the new syndrome in that Amish microcephaly is typically diagnosed at the second trimester (compared to the third trimester in our patients) and is associated with arrest of brain development *in utero*(Kelley et al., 2002; Siu et al., 2010).

PHENOTYPIC CHARACTERIZATION

Families A & B

Patients were born at term with a small head circumference (at least two standard deviations below average). From early infancy they showed feeding difficulties, jitteriness, and increased disabling spastic tone, followed by evolution of intractable infantile spasms around the age of three months. The spasms were replaced by frequent myoclonic and tonic seizures, partially responsive to anticonvulsant therapy. By the age of one year, the children failed to reach significant milestones, showed spastic quadriparesis, profound ID, and cortical blindness and had a head circumference seven standard deviations below average. Physical examination was remarkable for mild dysmorphic features including receding forehead, big fleshy ears and relatively big hands and feet. Electroencephalogram (EEG) evolved from burst suppression pattern at three months to multiple independent spike foci (MISF) on a slow background. Visual and auditory evoked potentials (VEP, BERA), as well as electroretinogram (ERG), were normal. Brain CT at two months of age showed cortical atrophy without calcifications. Magnetic resonance imaging (MRI) at the age of three months showed diffuse cerebral atrophy, enlarged extra-ventricular spaces with normal size cerebellum and brainstem and at the age of 18 months, progressive cortical and subcortical atrophy with delayed myelination, moderately enlarged lateral ventricles and thin corpus callosum. The brain stem was small, while the cerebellum was only very mildly affected (Figure S1B (ii)). In each of the families one pregnancy was terminated due to arrest of head growth detected by a fetal ultrasound. In the aborted child from family A, a fetal brain MRI was also performed, which identified bilateral cortical dysplasia and cerebellar hypoplasia, both of which were confirmed by autopsy.

Family C

The patients were three siblings born to a consanguineous Bangladeshi couple in good health. An older sister is unaffected. The parents are second cousins in that the mother's maternal grandmother and the father's maternal grandmother were siblings.

Patient C.II.1. The couple's first child, a male, was born at term following an uncomplicated pregnancy. Delivery was by C-section due to thick meconium as well as fetal distress. His APGAR score were 5 and 8 at 1 and 5 minutes respectively, his birth weight was 3400 g (50^{th} centile) and his head circumference (OFC) was 30.5 cm (-3.5SD). He was noted to be jittery during the first hour of life with episodes of hyperekplexia. He required oxygen at birth but quickly was weaned. EEG recording at 9 days of age was moderately abnormal due to disorganized and discontinuous background. No epileptiform discharges were seen. Initial MRI showed left transverse sinus

thrombosis and cerebral dysgenesis and renal ultrasound showed echogenic kidneys. He was treated with anticoagulants and a CT scan venography at 2 months of age showed that the thrombus cleared. He had no developmental milestones and showed feeding difficulties with episodes of aspirations for which a G-tube was inserted. Repeat brain MRI revealed an immature brain with delayed myelination as well as a left transverse sinus thrombosis. The infant continued having tremor, persistent hyperekplexia and was discharged from the hospital at a month of age only to be re-admitted at 3.5 months of age with respiratory failure. He was intubated and ventilated but multiple attempts at extubation over the course of 3.5 weeks failed due to central respiratory drive failure. Given the infant's futile outlook, the infant life support was withdrawn at 4 months of age. Investigation including chromosome analysis, metabolic work-up and studies for congenital infections showed no abnormalities. The family declined both autopsy and DNA banking.

The couple's second pregnancy resulted in a healthy daughter following an uneventful pregnancy and delivery. At 8 years of age she has no health or developmental issues.

Patient C.II.3. The couple's third pregnancy was followed closely and chorionic villi sampling (CVS) for maternal age revealed a normal male karyotype (46,XY). Serial ultrasounds at 19, 22, 26, and 32 weeks gestation all revealed normal head size at each gestational age. Delivery was by repeat caesarean section at 39 weeks gestation. Birthweight was 3520g (50^{th} centile) and OFC was 33 cm (-1SD/-2SD). Shortly after birth he developed jittery seizure-like movements and hyperekplexia mirroring those of his late brother. Extensive investigation including plasma amino acids [asparagine value was 12 mmol/L after birth and 17 mmol/L at 2 months (normal 16-21 mmol/L), urinary organic acids, plasma very long chain fatty acids, 7 dehydrocholesterol, transferrin isoelectric focusing, free and total carnitine, serum ceruloplasmin, blood CK, urine mucopolysaccharides and urine oligosaccharides were normal. Chromosome microarray analysis was normal. Initial EEG demonstrated intermittent right and left frontal sharp waves occurring independently of uncertain significance, possibly indicative of underlying cerebral dysfunction. No definitive seizure activity was noted. A repeat EEG done at a month of age was contaminated by a large amount of movement artifact. Within these limitations, the waking background activity did not show any definite abnormality, nor did a brief period of active sleep. Although not definitely abnormal, there were very frequent interictal sharp waves recorded independently over both frontopolar regions with a definite left sided predominance. No ictal epileptiform discharges were recorded. A repeat EEG at 2 months of age was abnormal with discontinuous and asynchronous background and positive Rolandic sharp waves seen over the left more than right hemisphere. No electrographic seizures were seen. Basal auditory evoked potential was normal, visual evoked potential and electroretinogram showed delayed cortical response by 45 msec and somatosensory evoked potential of the median nerve showed absent cortical response bilaterally. EMG was normal. Brain MRIs revealed volume loss of cerebral hemispheres and pons, with normal appearing cerebellum, delayed myelination of posterior limbs of internal capsule and dorsal brainstem, with mild restricted diffusion of both thalami and possibly basal ganglia. There was mildly elevated lactate peak on MRS and no imaging evidence of prenatal asphyxia. The findings were similar to the MRI findings performed on his late brother. At 2 months of age he was noted to have right hemidiaphragm palsy and had increasing respiratory failure. He developed hypothermia and hypercapnia and was removed from respiratory support at 3 months of age.

Patient C.II.4. The couple's fourth pregnancy was again followed closely and CVS for maternal age revealed a normal male karyotype (46,XY). Fetal ultrasounds at 19, 28, and 30 weeks showed normal head growth. At 32 weeks a slight lag in OFC was noted, with progressive development of microcephaly seen at 32, 34 and 35 weeks gestation by ultrasound. The baby was born at 35.7 weeks gestation via repeat C-section. The APGAR scores were 9 and 9 at 1 and 5 minutes respectively. Birth weight was 3230 g (50^{th} centile), birth length was 51.5 cm (50-97 centile) and OFC was 32 cm (-2SD). At 6 hours after birth, he was noted to have abnormal movements with jitteriness and hyperekplexia. He was initially intubated but extubated at 2 days of age and was noted to have stridor. He continued having seizure episodes with back arching and apnea and was treated with clonazepam and phenobarbital. EEG on his first day showed discontinuous background with longer interburst interval than appropriate for age with occasional positive and negative sharp waves over the left central and temporal head regions. There were occasional runs of theta and alpha rhythm of unknown significance. No seizures were captured during this recording. Brain MRI showed microcephaly, delayed myelination and under development of the brain with brainstem hypoplasia. The findings were similar to the MRIs done on the previous siblings. Plasma amino acids and urine organic acids were normal. The anticonvulsive treatment resulted in decrease in his jitteriness and he did not have respiratory problems apart from stridor, which was attributed to laryngomalacia. He was orally fed with frequent vomiting and continued having tremor and jitteriness although this decreased with time. He was transferred to a palliative care facility and died at 6 months of age.

Family D

The patients were three brothers born to a nonconsanguineous French-Canadian couple in good health. An older sister is unaffected.

SUPPLEMENTAL INFORMATION

Deficiency of asparagine synthetase causes congenital microcephaly and a progressive form of encephalopathy.

Patient D.II.1. The pregnancy and neonatal period were considered normal but on the first routine home visit by a nurse at 5 days of age, he was found to have irregular breathing, rectal temperature of 34.6° to have poor suction at feeds. He was examined in a local center and transferred to CHU Sainte-Justine where he was intubated and became respirator-dependent. He was microcephalic (31.5 cm; -2.5SD) with central hypotonia and increased tone in the legs and tremulous movements of the extremities. Visceral examination was normal. Glycemia, blood pH, transaminases, renal function were normal. Fasting plasma amino acids showed asparagine 11 µmol/L (normal range, 31 to 56). Urine organic acids and plasma very long chain fatty acids were interpreted as normal. Transferrin isofocalization was normal. MECP2 gene sequencing and deletion analysis were normal. Cerebral magnetic resonance imaging (MRI) showed microcephaly with reduced gyration. He was extubated and died rapidly thereafter of respiratory failure, aged 9 days. Neuropathological examination revealed microcephaly, although the gyral pattern was preserved grossly on external examination. There was cortical dysgenesis (nests of cells in the subpial region and multiple thin layers of nuclei in the cortex, thinner and more numerous than normal). Also present were absence of the bulbar arcuate nucleus, marked periventricular leukomalacia; and marked gliosis. The visceral examination was normal.

Patient D.II.2. The patient was born after a normal pregnancy at 39 5/7 weeks by spontaneous vaginal delivery. Fetal MRI at 31.5 weeks gestation and fetal ultrasound at 35 weeks, were normal. On neonatal examination, jerky and tremulous movements and limb hypertonia were noted. Body temperature was repeatedly normal. Head circumference was 31 cm (-3SD). At 4 days of age an EEG showed deficient electrical activity with bursts of activity with spike activity maximal in the right fronto-centro-temporal regions. Cerebral MRI at 4 days of age revealed a reduction of the normal gyral pattern. The opercularisation of the sylvian fissure corresponded to that of a 34 week old child (at a chronological age of 39 weeks). There was a diffuse hyposignal on T1 imaging, demonstrating a slowness of myelination. The parieto-occipital horns were prominent, especially on the left. The subarachnoid space was prominent. Plasma amino acids were normal including asparagine (55 µmol/L; normal, 31-56), as were urine organic acids, transferrin isofocusing, analysis of subtelomeres and ARX gene sequencing. Ophthalmologic consultation revealed cortical blindness. At age 9 months, partial motor convulsions were reported and focal epileptic activity was seen on EEG; control was achieved with carbamazepine. Examination at 10 months showed a nondysmorphic child with an absence of motor development and cranial circumference of 40 cm (<3%). He reacted to noise but showed no ocular pursuit. Divergent strabismus, axial hypotonia and limb hypertonia and hyperreflexia were present. The lower limbs were more severely affected than the upper. He died at age 11 months following an upper respiratory infection associated with respiratory acidosis (pCO2, 120; pH, 7.03) and hypothermia (30° C). At autopsy, neuropathology confirmed microcephaly with severe mesial temporal sclerosis and neuronal loss in regions CA3, CA4 and CA1, dysplasia of the olivary nucleus. The spinal cord showed hydromelia with secondary degeneration of motor neurons and reactive gliosis.

Patient D.II.3*.* The pregnancy was initially normal. Fetal ultrasound was normal at 25 weeks of gestation. Placental abruption with fetal distress occurred at 33 weeks, and emergency cesarean section was performed. Apgar scores were 4 at one minute, 7 at 5 minutes and 10 at 10 minutes. Birth weight was 2160 g (50-75%), length 46 cm (75%) and head circumference 30 cm (25^{th} centile). Although the patient initially cried vigorously, he showed hypoventilation within hours of birth. Respiratory distress syndrome was diagnosed clinically and on thoracic radiographs. He was intubated. Because of apneas he was treated with caffeine on day two. After resolution of his pulmonary disease, attempts to wean him from continuous positive airway pressure failed because of the development of apnea, cyanosis and bradycardia. Tremulous movements of the extremities were noted. He was transferred to CHU Sainte-Justine on day 6. Convulsions were noted on day 8. He was extubated at 3 weeks of age. At that time he could ingest adequate amounts of formula orally. His head circumference at one month of age was 30.2 cm and at 10 months, 39.5 cm (<3%). His subsequent clinical course was similar to that of patient 2. His convulsions were controlled by small doses of Phenobarbital. He died at age 12 months of respiratory insufficiency secondary to a respiratory infection, associated with hypothermia.

Haplotype prediction

To determine if the p.F362V *ASNS* variant is always found on the same haplotype, all high confidence SNVs (coverage ≥10, ≥5 reads supporting the variant, SNV quality ≥30, SNV consensus ≥30) on chromosome 7 were collected from each of the three exome-sequenced patients (Families A and B). Next, the regions on either side of the *ASNS* variant were examined to find the boundaries of the homozygous stretches containing the *ASNS* variant in each individual. Finally, the SNVs in this region were compared across samples to obtain the largest possible haplotype that was shared by all three affected patients. This estimated haplotype is approximately 1.2 Mb (build 36, Chr7: 97322654-98488035) and is tagged by 16 SNVs (Table S6).

These 16 SNVs were also assessed in the 261 sequenced controls. The genotype for each of these SNVs was input into the fastPHASE program[22] in order to infer the phase of these variants in each control sample. Only 17 controls had all 15 SNVs (the *ASNS* variant at the outer boundary was not found in any controls), and the majority of these variants were found in heterozygous form. Of the 522 possible haplotypes, fastPHASE determined that 2 haplotypes were identical to the *ASNS* haplotype (excluding the *ASNS* variant itself) when the individual haplotype error was minimized, and 4 haplotypes were identical to the *ASNS* haplotype (again, excluding the *ASNS* variant

itself) when switching error was minimized. All 4 of these control samples are self-identified as Caucasian.

Homozygosity mapping

To identify all potentially overlapping homozygous stretches between the families A and B, we used the exome-sequence data to detect homozygous regions present in these three cases. The largest homozygous region seen in all three case genomes was ~3 Mb and included the *ASNS* gene. The average size of the remaining shared homozygous regions (n=169), found in these three case genomes, was 131.4 Kb. The sequenced patients from families A and B have an average of 90% of bases covered across the protein-coding portions of the genes in the shared homozygous regions (Table S5). This analysis increases our confidence that the *ASNS* variant is the causal variant associated with the observed phenotype.

We used all identified high-quality single nucleotide variants to perform homozgyosity mapping. The SNVs in all three of the cases were analyzed using the PLINK "homozygosity mapping" tool(Purcell et al., 2007). This algorithm considers sliding windows across the genome and screens for homozygous variants in those regions. To account for the nonrandom spacing of SNVs in the exome data and to detect such regions with high sensitivity, very generous thresholds were applied as outlined below.

The default values provided by PLINK were designed for analysis from dense SNP maps. However, here we were analyzing the SNVs identified by exome-sequencing. Thus before proceeding, all SNVs were filtered for those with very high quality (coverage ≥10, ≥5 reads supporting the variant, SNV quality ≥30, SNV consensus ≥30). We defined a "window" as 10 SNPs within a 1,000 Kb window. One heterozygous SNV was allowed in a window. A homozygous segment was then defined as a region with 10 SNVs in a 1 Kb window.

This analysis identified 1,532 homozygous regions (≥1 Kb) in total, with approximately 500 in each case genome. The two siblings from family B had 341 regions that overlapped by at least 500 base pairs. These regions were then compared to the homozygous regions identified in the third unrelated patient from family A. There were 169 homozygous regions that overlapped by at least 500 bp and they were found in all three case genomes.

The exome data were re-examined by focusing only on regions of homozygosity. This analysis revealed that the case genomes contained only 20 rare and plausibly functional sequence variants (predicted homozygote frequency of ≤3% in our sequenced control genomes) in these homozygous regions. The majority of these 20 variants were found in only one of the three case genomes. There was only one plausibly functional variant (non-synonymous) present in two of the three case genomes, however this variant was very common (control MAF of 0.13). Importantly, only the *ASNS* variant was present in all three case genomes from families A and B.

Homozygosity mapping was also done in family C at the McGill University Genome Quebec Innovation Center (Montreal, Canada). Briefly, genomic DNA (~2.5µg) from the blood of the two affected siblings (C:II.3 and II.4) was used to perform whole-genome genotyping using the Illumina 660 Quad Chip (Infinium HD). PLINK (v.1.06)(Purcell et al., 2007) was used to identify shared regions of homozygosity with a size of >1Mb.

ASNS in population controls

We looked in the CHGV dataset of 4,845 high-density genome-wide SNP genotyped controls and found no copy number variations (CNVs), as predicted by PennCNV, which overlapped the *ASNS* gene (data not shown). Additionally, only one CNV in this region is reported in the Database of Genomic Variants (http://projects.tcag.ca/variation/). The involvement of *ASNS* in this phenotype would have been refuted, if homozygous deletions encompassing this gene had been observed in this CNV data. Also, *ASNS* has a halopinsufficeny score of 0.551(Huang et al., 2010).

ASNS conservation and mutation locations in the folded ortholog

An examination of the *E. coli* ortholog structure (pubmid:10587437) reveals that the inferred p.A6E position is located in the N-terminal domain (which is responsible for glutamine hydrolysis), that faces a pocket identified as the glutamine binding site (pubmid:10587437, Fig. 3b). The inferred p.F362V position is located on the C-terminal domain, near the AMP binding site (Fig. 3b). The inferred p.R550C position is located at the distal end of the C-terminus which is disordered in the E. coli ortholog and thus the crystallographic structure is not available. However, this region is in the interface between the N-terminal and C-terminal domains and it might play a role in binding the aspartate substrate (pubmid:10587437). Additionally, the predicted deleterious effect of these mutations on the protein functionality (Table 2) supports the putative destabilization observed in our heterologous expression experiment, as well as the functionally important disposition of the mutated residues in the homologous 3D structure.

SUPPLEMENTAL INFORMATION

Deficiency of asparagine synthetase causes congenital microcephaly and a progressive form of encephalopathy.

Mouse behavioral testing

Mouse behavioral testing: overview

No genotype differences were discerned for spontaneous locomotor activity in the open field (Figure S5A (i)) or in the overall time spent in movement (Figure S5B (i)). Similarly, no genotype distinctions were seen for anxiety-like behavior in the open field (Figure S5B (ii)) or in the light-dark emergence test (Figure S5B (iii-iv)). In the accelerating rotorod test, $Asns^{+/-}$ and $Asns^{-/-}$ mice stayed on the rotorod longer than CONT mice over the first three trials of testing (Figure S5A (ii)). However, CONT mice showed motor learning across trials, whereas a ceiling effect probably precluded seeing this change in performance in the mutant mice. Episodic memory was examined in the novel object recognition test where short- (STM) and long-term memory (LTM) were evaluated(Rampon et al., 2000). In the STM test, $Asns^{+/-}$ and $Asns^{-/-}$ mice showed no preference for either the novel or familiar object. In the test for LTM, the $Asns^{-/-}$ mice failed to demonstrate a preference for either object. By comparison, CONT and $Asns^{+/-}$ animals preferred the novel object; however, LTM was still reduced in the $Asns^{-/-}$ mice (Figure S5A (iii)). It should be emphasized that the deficits in STM or LTM by the mutants was not related to the total time spent with the objects or to the total numbers of object contacts (Figure S5B (v-vi)). Collectively, these data indicate that $Asns^{-/-}$ mice are impaired in both STM and LTM. By contrast, there is some sparing of LTM in the $Asns^{+/-}$ animals, suggesting that memory consolidation is delayed in these mutants.

Mouse behavioral testing: methods

Adult male and female B6NTac (Taconic Labs, Hudson, NY) served as controls and were tested with the heterozygous and homozygous mutant mice (B6NTac;B6N-$Asns^{tm1a(EUCOMM)Wtsi}$/H; European Mutant Mouse Archive, Munich, Germany). Adult CONT, $Asns^{+/-}$, and $Asns^{-/-}$ mice were housed under controlled temperature and humidity conditions under a 14:10 h light:dark cycle (light onset 0800 h) with food and water provided ad *libitum*. All behavioral assessments were conducted during the light cycle between 1000 and 1700 h. Mice were tested in following order with 3-5 days interposed between tests: light-dark emergence, open field, rotorod, and novel object recognition as described(Carlson et al., 2011). All procedures were approved by the Duke University Institutional Animal Care and Use Committee and were in conducted accordance with NIH guidelines for the care and use of laboratory animals.

All behavioral data are presented as means and SEM and were analyzed with SPSS 20 (IBM North America, New York, New York) using ANOVA (open field, light-dark emergence test), repeated measures ANOVA (RMANOVA; rotarod, novel object recognition test), and the Kruskall-Wallis test for rank-ordered data (percent increases in performance during rotorod testing). Bonferroni corrected pair-wise comparisons were used for *aposteriori* comparisons where a $p<0.05$ was considered significant.

The mice were tested in the light-dark emergence test for 5 min and were monitored with Med-PC IV software (Med-Associates, St. Albans, VT); the open field data were collected over 30 min with Versamax software (Accuscan Instruments, Columbus, OH); the accelerating rotorod data were collected over 5 min with Med-Associates rotorod software; and the novel object recognition testing was conducted in Plexiglas arenas with mouse-friendly objects over 10 min and analyzed with TopScan software (Clever Sys Inc., Reston, VA). Preference scores in the novel object recognition test were calculated by subtracting the total time spent with the novel object from the total time spent with the familiar object during each test, and divided by the total time spent with both objects. Positive scores indicated a preference for the novel object, negative scores a preference for the familiar object, and scores approaching zero indicated no preference for either object.

Mouse behavioral testing: additional results

In the open field an ANOVA revealed no significant genotype differences for spontaneous distance traveled (Figure S5A (i)), time spent in overall movement (Figure S5B (i)), or distance moved in the center of the open field (Figure S5B (ii)).

In the rotorod test, a RMANOVA for latency to fall for the within subjects test found the main effect of test-trial to be significant [$F_{(3,66)}=7.832$, $p<0.001$] and the between subjects test revealed a significant genotype effect [$F_{(2,22)}=5.174$, $p<0.014$]. Although the genotype by test-trial interaction was not significant, inspection of the Figure S5A (ii) indicated that the genotypes were differentially responding to the task. When data were expressed as the percent change in latency to fall from the first to last trials; CONT mice showed a 183% increase in motor learning over testing, whereas a small enhancement 25% was observed in the $Asns^{+/-}$ animals and $Asns^{-/-}$ mice had an increase of 51%. A Kruskal-Wallis test for rank-ordered data found a significant difference between the three genotypes [$H_{(2,22)}=6.281$, $p<0.043$]; confirming that performance of the CONT animals was superior to that of the $Asns^{+/-}$ and $Asns^{-/-}$ mice.

In the light-dark emergence test, ANOVA for the latency to emerge from the darkened chamber into the lighted chamber (Figure S5B (iii)) and the time spent in the lighted chamber (Figure S5B (iv)) were not significantly different among genotypes.

In the novel object recognition test, a RMANOVA reported a significant effect of test-session [$F_{(2,44)}$=11.209, p<0.001] and a significant test-session by genotype interaction [$F_{(4,44)}$=6.178, p<0.043]. Bonferroni corrected pair-wise comparisons for the STM test revealed that $Asns^{+/-}$ and $Asns^{-/-}$ mice had significant lower preference scores for the novel object than CONT animals (ps<0.039); preference scores between the mutants did not differ (Figure S5A (iii)). In the test for LTM, preference scores were increased for the $Asns^{+/-}$ mice relative to their performance in the STM test. However, their scores were still significantly lower (p<0.046) than those for CONT animals. By comparison, $Asns^{-/-}$ mice continued to show no object preference and their scores were significantly lower than those for the $Asns^{+/-}$ and CONT animals (ps<0.001). Despite differences in the preference scores, the genotypes of mice did not differ according to time spent exploring the objects (Figure S5B (v)) or total contacts with the objects (Figure S5B (vi). These data indicate that memory function is severely impaired in the $Asns^{-/-}$ mice and is less deficient in the $Asns^{+/-}$ animals.

SUPPLEMENTAL REFERENCES

Bilguvar, K., Öztürk, A.K., Louvi, A., Kwan, K.Y., Choi, M., Tatli, B., Yalnizoğlu, D., Tuysuz, B., Çağlayan, A.O., Gökben, S., et al. (2010). Whole-exome sequencing identifies recessive WDR62 mutations in severe brain malformations. Nature *467*, 207–210.

Carlson, B.R., Lloyd, K.E., Kruszewski, A., Kim, I.-H., Rodriguiz, R.M., Heindel, C., Faytell, M., Dudek, S.M., Wetsel, W.C., and Soderling, S.H. (2011). WRP/srGAP3 facilitates the initiation of spine development by an inverse F-BAR domain, and its loss impairs long-term memory. The Journal of Neuroscience : the Official Journal of the Society for Neuroscience *31*, 2447–2460.

Cox, J., Jackson, A.P., Bond, J., and Woods, C.G. (2006). What primary microcephaly can tell us about brain growth. Trends Mol Med *12*, 358–366.

Guernsey, D.L., Jiang, H., Hussin, J., Arnold, M., Bouyakdan, K., Perry, S., Babineau-Sturk, T., Beis, J., Dumas, N., Evans, S.C., et al. (2010). Mutations in Centrosomal Protein CEP152 in Primary Microcephaly Families Linked to MCPH4. The American Journal of Human Genetics *87*, 40–51.

Hart, C.E., Race, V., Achouri, Y., Wiame, E., Sharrard, M., Olpin, S.E., Watkinson, J., Bonham, J.R., Jaeken, J., Matthijs, G., et al. (2007). Phosphoserine aminotransferase deficiency: a novel disorder of the serine biosynthesis pathway. The American Journal of Human Genetics *80*, 931–937.

Horowitz, B., Madras, B.K., Meister, A., Old, L.J., Boyes, E.A., and Stockert, E. (1968). Asparagine synthetase activity of mouse leukemias. Science *160*, 533–535.

Huang, N., Lee, I., Marcotte, E., Hurles, M., and Schierup, M. (2010). Characterising and Predicting Haploinsufficiency in the Human Genome. PLoS Genet.

Hubbard, T.J.P., Aken, B.L., Ayling, S., Ballester, B., Beal, K., Bragin, E., Brent, S., Chen, Y., Clapham, P., Clarke, L., et al. (2009). Ensembl 2009. Nucleic Acids Res *37*, D690–D697.

Kaindl, A.M., Passemard, S., Kumar, P., Kraemer, N., Issa, L., Zwirner, A., Gerard, B., Verloes, A., Mani, S., and Gressens, P. (2010). Many roads lead to primary autosomal recessive microcephaly. Progress in Neurobiology *90*, 363–383.

Kelley, R.I., Robinson, D., Puffenberger, E.G., Strauss, K.A., and Morton, D.H. (2002). Amish lethal microcephaly: A new metabolic disorder with severe congenital microcephaly and 2-ketoglutaric aciduria. Am J Med Genet *112*, 318–326.

Langmead, B., Trapnell, C., Pop, M., and Salzberg, S.L. (2009). Ultrafast and memory-efficient alignment of short DNA sequences to the human genome. Genome Biol *10*, R25.

Nicholas, A.K., Khurshid, M., Désir, J., Carvalho, O.P., Cox, J.J., Thornton, G., Kausar, R., Ansar, M., Ahmad, W., Verloes, A., et al. (2010). WDR62 is associated with the spindle pole and is mutated in human microcephaly. Nature Publishing Group *42*, 1010–1014.

Purcell, S., Neale, B., Todd-Brown, K., Thomas, L., Ferreira, M.A.R., Bender, D., Maller, J., Sklar, P., de Bakker, P.I.W., Daly, M.J., et al. (2007). PLINK: a tool set for whole-genome association and population-based linkage analyses. Am J Hum Genet *81*, 559–575.

Quinlan, A.R., and Hall, I.M. (2010). BEDTools: a flexible suite of utilities for comparing genomic features. Bioinformatics *26*, 841–842.

Rampon, C., Tang, Y.P., Goodhouse, J., Shimizu, E., Kyin, M., and Tsien, J.Z. (2000). Enrichment induces structural changes and recovery from nonspatial memory deficits in CA1 NMDAR1-knockout mice. Nature Publishing Group *3*, 238–244.

Siu, V.M., Ratko, S., Prasad, A.N., Prasad, C., and Rupar, C.A. (2010). Amish microcephaly: Long-term survival and biochemical characterization. Am J Med Genet *152A*, 1747–1751.